Relativistic parameterizations of neutron matter and implications for neutron stars

Nadine Hornick,[1] Laura Tolos,[1,2,3,4,*] Andreas Zacchi,[1,†] Jan-Erik Christian,[1,‡] and Jürgen Schaffner-Bielich[1,§]

[1]*Institut für Theoretische Physik, Goethe Universität, Max-von-Laue-Straße 1, D-60438 Frankfurt, Germany*
[2]*FIAS, Goethe Universität, Ruth Moufang Str 1, D-60438 Frankfurt, Germany*
[3]*Institute of Space Sciences (ICE, CSIC), Campus UAB, Carrer de Can Magrans, 08193 Barcelona, Spain*
[4]*Institut d'Estudis Espacials de Catalunya (IEEC), 08034 Barcelona, Spain*

We construct parameter sets of the relativistic mean-field model fitted to the recent constraints on the asymmetry energy J and the slope parameter L for pure neutron matter. We find cases of unphysical behavior, i.e., the appearance of negative pressures, for stiff parameter sets with low values of the effective mass m^*/m. In some cases the equation of state of pure neutron matter turns out to be outside the allowed band given by chiral effective field theory. The mass-radius relations of neutron stars for all acceptable parameter sets shows a maximum mass in excess of $2M_\odot$ being compatible with pulsar mass measurements. Given the constraints on the model in the low-density regime coming from chiral effective theory, we find that the radius of a $1.4M_\odot$ neutron star is nearly independent of the value of L. This is in contrast to some previous claims for a strong connection of the slope parameter with the radius of a neutron star. In fact, the mass-radius relation turns out to depend only on the isoscalar parameters of symmetric matter. The constraints of GW170817 on the tidal deformability and on the radius are also discussed.

I. INTRODUCTION

Neutron stars have received a lot of attention over the years [1–3], especially since the detection of gravitational waves from the neutron star binary merger GW170817 [4]. The two most important properties of neutron stars, maximum mass and radius, are still a matter of intense analysis since they are linked to the physics of their interior, which is nowadays an open question.

It is now established that neutron stars, usually observed as pulsars, can have masses of up to $2M_\odot$ [5–7]. The precise determination of neutron star radii is still an ongoing process. Model-dependent constraints on the radius have been derived by fits to low mass quiescent x-ray binary data and thermonuclear bursts, sometimes with conflicting results [8–24]. Recent analysis of tidal deformabilities from the neutron star merger seen in gravitational waves, GW170817, however, were able to set limits on the radius of a $M = 1.4M_\odot$ neutron star in the range of $R = 12$–13.5 km based on statistical approaches [4,25–28]. Future high-precision x-ray space missions, such as the ongoing NICER (Neutron Star Interior Composition ExploreR) [29] and the future eXTP (Enhanced X-ray Timing and Polarimetry Mission) [30], will improve the situation by simultaneous measurements of masses and radii with higher accuracy [31]. Limits on neutron star radii are also expected to be refined by future detections of gravitational-wave signals from neutron star mergers.

The mass and radius of neutron stars strongly depend on the properties of matter in their interior, which is described by means of the equation of state (EoS). Indeed, the determination of the EoS is a field of extensive and active research. Among the different approaches to obtain the EoS, the relativistic mean-field (RMF) models [32–37] have been widely used for describing the interior of neutron stars based on fits to nuclear ground-state properties and/or on fitting the parameters of the model directly to properties of nuclei, such as masses, charge radii, and surface thickness. Yet it is far from a trivial task to generate an EoS that respects the properties of nuclear matter and nuclei as well as describes pure neutron star matter. Recall that it is an extrapolation of ≈ 18 orders of magnitude from the radius of a nucleus to the radius of a neutron star [38,39]. For densities $\rho \leqslant 4 \times 10^{11}$ g/cm^3 neutron stars are expected to have a outer crust consisting of a lattice of neutron-rich nuclei. Up to densities of about $\rho \approx 10^{14}$ g/cm^3, the inner crust consists of a lattice of nuclei immersed within a neutron liquid. At higher densities the outer core is liquid neutron-rich matter, consisting of a liquid of neutrons with a small admixture of protons and electrons. For the inner core, probably starting at twice saturation density, i.e., at $\rho \geqslant 5 \times 10^{14}$ g/cm^3, one may speculate about exotic phases of matter, such as hyperon matter (see Ref. [40] for a review) or quark matter (see, e.g., Refs. [41–45]).

In this paper we present relativistic parameter sets for the EoS of the interior of neutron stars that fulfill the $M \geqslant 2M_\odot$ neutron star mass constraint from the observations of pulsars and the radius constraint from GW170817 of $R = 12$–13.5 km, while fulfilling the saturation properties of nuclear matter. Moreover, we impose further constraints on

*tolos@th.physik.uni-frankfurt.de
†zacchi@astro.uni-frankfurt.de
‡christian@astro.uni-frankfurt.de
§schaffner@astro.uni-frankfurt.de

the EoS for neutron matter coming from chiral effective field theory (χEFT) [46]. These constraints are met by simultaneously fitting the isoscalar couplings to saturation properties, while allowing for variations of the isovector parameters and the effective nucleon mass (m^*/m) so as to reproduce the symmetry energy (J) and its slope (L) within reasonable theoretical and experimental limits [3,11,47–50].

We find that the values of the symmetry energy and its slope that allow for a physical solution for the neutron matter EoS compatible with χEFT depend on the value of the nucleon effective masses at saturation density. We also observe that the behavior of both the maximum mass and the radius of neutron stars is dominated by the effective nucleon mass. The restricted range of L values coming from χEFT constraints does not allow for an appreciable variation of the radius, while being not relevant for the determination of the maximum mass. All parameter sets result in maximum neutron star masses in excess of the $2M_\odot$ limit. Large values of the effective nucleon mass induce small neutron star radii, so that effective nucleon masses of $m^*/m > 0.60$ are needed in order to have radii compatible with the recent upper limit of the tidal deformabilities and radii from GW170817.

The paper is organized as follows. In Sec. II we present the model Lagrangian and derive the corresponding equations of motion. We determine the parameters of the model in Sec. III, while presenting our results for the EoS, mass-radius relation, and dimensionless tidal deformability in Sec. IV. Our conclusions are summarized in Sec. V. The tables with the isoscalar and isovector parameters of the model can be found in Appendix A.

II. THEORETICAL FRAMEWORK

The properties of the nuclear EoS and of finite nuclei can be described within the RMF model, using a contemporary formulation of the Lagrangian density of the theory [32–37]. In this framework, the interactions among nucleons (N), three mesons (σ, ω, and ρ), and the photon can be depicted by the effective Lagrangian for the interaction

$$\mathcal{L}_{\text{int}} = \sum_N \bar{\Psi}_N \left[g_\sigma \sigma - g_\omega \gamma^\mu \omega_\mu - \frac{g_\rho}{2} \gamma^\mu \vec{\tau} \vec{\rho}_\mu - q_N \gamma^\mu A_\mu \right] \Psi_N$$
$$- \frac{1}{3} b\, m (g_\sigma \sigma)^3 - \frac{1}{4} c (g_\sigma \sigma)^4$$
$$+ \Lambda_\omega \left(g_\rho^2 \vec{\rho}_\mu \vec{\rho}^{\,\mu} \right) \left(g_\omega^2 \omega_\mu \omega^\mu \right) + \frac{\zeta}{4!} \left(g_\omega^2 \omega_\mu \omega^\mu \right)^2, \quad (1)$$

where Ψ_N indicates the Dirac field for the nucleons ($n =$ neutron and $p =$ proton), m is the average nucleon mass, while σ, ω_μ, and $\vec{\rho}_\mu$ are the mesonic fields and A_μ the photon field. Also, q_N is the charge of the nucleon and $\vec{\tau}$ indicates the Pauli matrices.

The g_σ and g_ω couplings of the isoscalar σ and ω mesons to the nucleon determine the energy per particle and density of the ground state of nuclear matter. The g_ρ coupling of the isovector ρ meson to the nucleon is important for the nuclear symmetry energy. Moreover, the σ-meson self-interactions, with the b and c couplings, allow for a quantitatively successful description of nuclear matter and finite nuclei, as they

soften the EoS at moderate densities giving rise to a realistic incompressibility of nuclear matter [51–53]. The mixed interaction among ω and ρ, Λ_ω, models the density dependence of the nuclear symmetry energy [36,39,54], influencing the neutron radius of heavy nuclei and, presumably, neutron star radii. Finally, the quartic self-coupling ζ of ω softens the EoS at high densities [33,39,55], affecting the maximum mass of neutron stars.

Given the Lagrangian density of Eq. (1), one can derive the equation of motion for each particle. Nucleons satisfy the Dirac equation

$$\left(i\gamma^\mu \partial_\mu - q_N \gamma^\mu A_\mu - m^* - g_\omega \gamma^0 \omega_0 - \frac{g_\rho}{2} \tau_{3N} \gamma^0 \rho_{30} \right) \Psi_N$$
$$= 0,$$

with $\tau_{3p} = +1$ for the proton and the effective mass of the nucleon being

$$m^* = m - g_\sigma \sigma. \quad (2)$$

While the photon obeys the Poisson equation with the proton density being the source term, the mesonic equations of motion follow from the respective Euler-Lagrange equations. In the mean-field approach, the mesons are replaced by the mean-field expectation values, that is, $\bar{\sigma} = \langle \sigma \rangle$, $\bar{\omega} = \langle \omega^0 \rangle$, $\bar{\rho} = \langle \rho_3^0 \rangle$. Thus, the mesonic equations of motion read

$$m_\sigma^2 \bar{\sigma} + m\, b\, g_\sigma^3 \bar{\sigma}^2 + c\, g_\sigma^4 \bar{\sigma}^3 = g_\sigma n^s,$$
$$m_\omega^2 \bar{\omega} + \frac{\zeta}{3!} g_\omega^4 \bar{\omega}^3 + 2\Lambda_\omega g_\rho^2 g_\omega^2 \bar{\rho}^2 \bar{\omega} = g_\omega n, \quad (3)$$
$$m_\rho^2 \bar{\rho} + 2\Lambda_\omega g_\rho^2 g_\omega^2 \bar{\omega}^2 \bar{\rho} = \frac{g_\rho}{2} n_3.$$

The quantities $n^s = n_p^s + n_n^s$ and $n = n_p + n_n$ are the scalar and vector nuclear densities, respectively, whereas $n_3 = n_p - n_n$, all of them in terms of the proton and neutron densities, generically defined as

$$n_N^s = \frac{m^*}{2\pi^2} \left[E_{F_N} k_{F_N} - m^{*2} \ln \frac{k_{F_N} + E_{F_N}}{m^*} \right],$$
$$n_N = \frac{k_{F_N}^3}{3\pi^2}, \quad (4)$$

with $E_{F_N} = \sqrt{k_{F_N}^2 + m^{*2}}$, where k_{F_N} is the nucleon Fermi momentum.

With the above results, one can derive the energy density from the energy momentum tensor in the mean-field approximation:

$$\varepsilon = \sum_N \frac{1}{8\pi^2} \left[k_{F_N} E_{F_N}^3 + k_{F_N}^3 E_{F_N} - m^{*4} \ln \frac{k_{F_N} + E_{F_N}}{m^*} \right]$$
$$+ \frac{1}{2} m_\sigma^2 \bar{\sigma}^2 + \frac{1}{2} m_\omega^2 \bar{\omega}^2 + \frac{1}{2} m_\rho^2 \bar{\rho}^2 + \frac{1}{3} b\, m (g_\sigma \bar{\sigma})^3$$
$$+ \frac{1}{4} c (g_\sigma \bar{\sigma})^4 + \frac{\zeta}{8} (g_\omega \bar{\omega})^4 + 3\Lambda_\omega (g_\rho g_\omega \bar{\rho}\, \bar{\omega})^2. \quad (5)$$

The pressure can be obtained via

$$P = \sum_N \mu_N n_N - \varepsilon, \quad (6)$$

where the nucleonic chemical potential is given by

$$\mu_N = E_{F_N} + g_\omega \bar\omega + \frac{g_\rho}{2}\,\tau_{3N}\,\bar\rho. \tag{7}$$

III. CALIBRATION OF THE MODEL

In order to analyze the effect of the nuclear bulk properties of infinite nuclear matter on the mass and radius of neutron stars, one has to connect the coupling constants of the Lagrangian for the interaction in Eq. (1) with the nuclear matter properties. We follow the procedure described in Ref. [37], where the isoscalar and isovector coupling constants are fixed in terms of the different bulk parameters of infinite nuclear matter.

On the one hand, the isoscalar coupling constants (g_σ, g_ω, b, and c) are determined by fixing the saturation density n_0 as well as the binding energy per nucleon E/A, the incompressibility coefficient K and the effective nucleon mass m^*/m at saturation. In this work we take $n_0 = 0.15$ fm^{-3}, $E/A(n_0) = -16$ MeV, while the incompressibility is chosen to be $K(n_0) = 240$ MeV, based on Ref. [56] and within the accepted values reported in Ref. [3]. Moreover, the effective nucleon mass will be varied between $m^*/m = 0.55$ and 0.75. The values for the isoscalar coupling constants are given in Table II of the Appendix A for the different values of the effective nucleon mass. The remaining coupling constant ζ is set to zero, so as to produce the stiffest possible EoS at high densities. In our calculations, we take $m = 939$ MeV, $m_\omega = 783$ MeV, and $m_\sigma = 550$ MeV for the masses of the nucleon, ω and σ mesons, respectively. On the other hand, we explicitly show how the isovector couplings (g_ρ and Λ_ω) are determined as a function of the symmetry energy J and the slope of the symmetry energy at saturation L, summarizing the procedure of Ref. [37].

An analytical expression for the density-dependent symmetry energy is

$$S(n) = S_0(n) + S_1(n) = \frac{k_F^2}{6E_F} + \frac{g_\rho^2 n}{8m_\rho^{*2}},$$

$$\text{with } \frac{m_\rho^{*2}}{g_\rho^2} = \frac{m_\rho^2}{g_\rho^2} + 2\Lambda_\omega g_\omega^2 \bar\omega^2. \tag{8}$$

Here $S_0(n)$ and $S_1(n)$ are the isoscalar and the isovector parts of the density-dependent symmetry energy. Given that the isoscalar sector has been fixed, $S_0(n)$ and derivatives are known, while $S_1(n)$ is unknown as g_ρ and Λ_ω are not determined. We can use, however, the experimental knowledge on the symmetry energy at saturation density $J = S(n_0)$ as well as the slope $L = 3n_0(\frac{dS}{dn})_0$ to determine g_ρ and Λ_ω.

We start by writing J as

$$J = S(n_0) = J_0 + J_1,$$
$$J_0 = S_0(n_0) = \left(\frac{k_F^2}{6E_F}\right)_0, \tag{9}$$
$$J_1 = S_1(n_0) = \left(\frac{g_\rho^2 n}{8m_\rho^{*2}}\right)_0.$$

For a given m^*/m at n_0, we can compute J_0. Then, J_1 is also known as we fix J.

Moreover, the slope parameter L reads as

$$L = 3n_0\left(\frac{dS}{dn}\right)_0 = L_0 + L_1, \tag{10}$$

where

$$L_0 = 3n_0\left(\frac{dS_0}{dn}\right)_0 = 3n_0\left[\left(\frac{\partial S_0}{\partial n}\right) + \left(\frac{\partial S_0}{\partial m^*}\right)\left(\frac{\partial m^*}{\partial n}\right)\right]_0,$$
$$L_1 = 3n_0\left(\frac{dS_1}{dn}\right)_0 = 3n_0\left[\left(\frac{\partial S_1}{\partial n}\right) + \left(\frac{\partial S_1}{\partial \bar\omega}\right)\left(\frac{\partial \bar\omega}{\partial n}\right)\right]_0. \tag{11}$$

After a bit of algebra, it was shown in Ref. [37] that

$$L_0 = J_0\left\{1 + \frac{m^{*2}}{E_F^2}\left[1 - \frac{3n}{m^*}\left(\frac{\partial m^*}{\partial n}\right)\right]\right\}_0, \tag{12}$$

with

$$\left(\frac{\partial m^*}{\partial n}\right) = -\frac{m^*}{E_F}\left[\frac{m_{\sigma^*}^2}{g_\sigma^2} + \frac{\partial n^s}{\partial m^*}\right]^{-1}, \tag{13}$$

in terms of

$$\frac{m_{\sigma^*}^2}{g_\sigma^2} = \frac{m_\sigma^2}{g_\sigma^2} + 2bmg_\sigma\bar\sigma + 3cg_\sigma^2\bar\sigma^2,$$
$$\frac{\partial n^s}{\partial m^*} = \frac{1}{\pi^2}\left[\frac{k_F}{E_F}(E_F^2 + 2m^{*2}) - 3m^{*2}\ln\left(\frac{k_F + E_F}{m^*}\right)\right]. \tag{14}$$

The quantity L_0 is given exclusively in terms of isoscalar parameters, so it is known. As for L_1 [37]

$$L_1 = 3J_1\left[1 - 32\left(\frac{g_\omega^2}{m_\omega^{*2}}\right)g_\omega\bar\omega\Lambda_\omega J_1\right]_0, \tag{15}$$

with $m_\omega^* = m_\omega$, since $\zeta = 0$ [37]. Therefore, knowing L_0 and given L, L_1 is easily calculated and, hence, Λ_ω.

As for g_ρ, we use Eq. (15) for Λ_ω as well as Eqs. (8) and (9), so we find

$$\frac{g_\rho^2}{m_\rho^2} = \left[\frac{n}{8J_1} - 2\Lambda_\omega g_\omega^2\bar\omega^2\right]_0^{-1}. \tag{16}$$

The values for g_ρ and Λ_ω are given in Tables III and IV of Appendix A for $J = 30$ and $J = 32$, respectively, and for different values of L, such that $40 \leqslant L \leqslant 60$ MeV. The values of J and L are taken to be compatible with estimations coming from the analysis of a variety of nuclear data from terrestrial experiments, astrophysical observations, and theoretical calculations [3,11,47–50].

IV. EQUATION OF STATE, MASS-RADIUS, AND TIDAL DEFORMABILITY OF NEUTRON STARS

A. Constraints on the equation of state

As mentioned in the previous section, the EoS must fulfill certain nuclear matter properties at saturation density, as well as certain constraints of J and L. Moreover, we further restrict the possible EoSs by imposing that their behavior for neutron matter at densities around saturation density must be compatible with recent low-density constraints coming
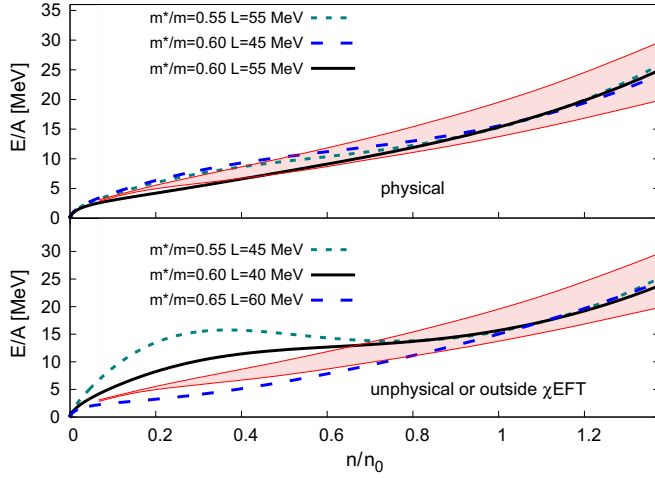
FIG. 1. EoS for neutron matter as a function of n/n_0 at $J = 30$ MeV for different values of the nucleon effective mass m^*/m and slope parameter L. The top panel display solutions within the χEFT allowed band that present no instabilities, while the bottom panel collects some solutions for the neutron matter EoS that are outside the χEFT band and/or present instabilities.

FIG. 3. Scatter plot of the slope parameter L and of the nucleon effective mass m^*/m for $J = 30$ MeV, where the unphysical solutions for neutron matter EoS (marked with a red plus sign), the solutions for neutron matter EoS outside the χEFT band (blue cross) and the physical solutions inside the χEFT region (green star) are indicated.

from the analysis of χEFT for densities up to 1.3 n_0 [46]. Thus, we examine the EoSs compatible with these constraints for neutron matter by varying the effective nucleon mass, which is a free parameter, within certain reasonable limits, between $m^*/m = 0.55$ and 0.75 [57]. Needless to say, we only allow for physical solutions, where neutron matter EoS always increases with density so that no unstable regions are present.

With all these restrictions, we show the neutron matter EoSs for $J = 30$ in Fig. 1 and for $J = 32$ in Fig. 2 by simultaneously changing L and m^*/m. The top panels in these figures correspond to solutions of the neutron matter EoS that are compatible with the allowed band region from χEFT (red shaded area) and present no instabilities, while the bottom panels show neutron matter EoSs that are outside the allowed χEFT and/or that are unphysical as they present
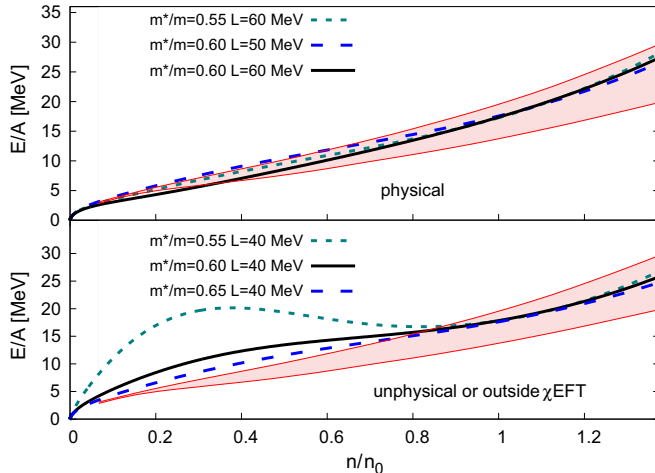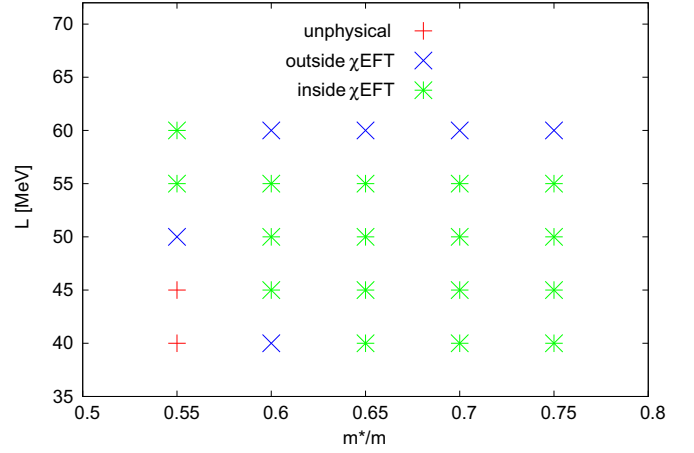
unstable regions. We observe that the physical solutions for neutron matter EoS require larger values for L as we increase J for a fixed m^*/m of 0.55 MeV and 0.60 MeV. We also find that as we take small values of L, such as $L = 40$ or $L = 45$, a too small effective nucleon mass induces the appearance of instabilities in the neutron matter EoS.

The previous conclusions can be extracted from Figs. 3 and 4, where the unphysical neutron matter EoS solutions (red plus sign), the solutions for the neutron matter EoS outside the χEFT band (blue cross), and the physical solutions inside the χEFT region (green star) are depicted indicating their corresponding L and m^*/m. These figures show a distinctive pattern for both values of J: it is more difficult to find a physical solution for the neutron matter EoS compatible with the χEFT results for small values for m^*/m and L at the same time. This is due to Hugenholtz-van-Hove theorem [52,58] that states that the binding energy per particle must be equal

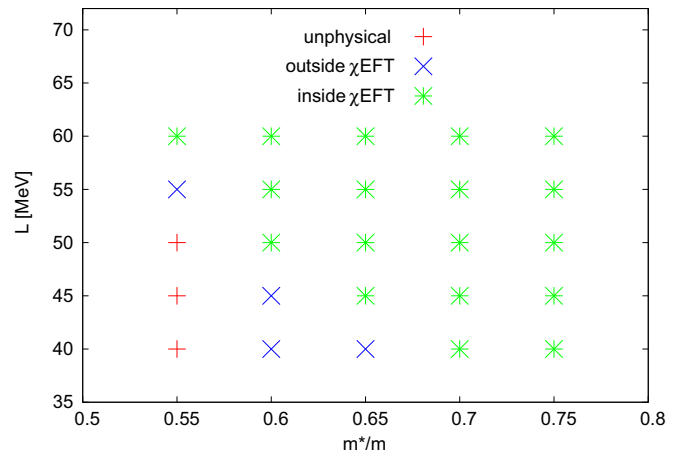
FIG. 2. The same as Fig. 2 but for $J = 32$.

FIG. 4. The same as Fig. 3 but for $J = 32$ MeV.

to the Fermi energy at saturation. Thus, the increase in the scalar potential (or reduction in the effective nucleon mass) will lead to bigger values for the ω field and, hence, to a stiffer EoS. Thus, a softening of the EoS induced by a small value of L competes with the stiffening of the EoS as we reduce the effective nucleon mass, leading to either a solution outside the band of χEFT or the appearance of unstable solutions below saturation density. Also, we find that it is not possible to lower the value of J from 32 MeV to 30 MeV for a fixed m^*/m in order to obtain physical solutions of the neutron matter EoS that fulfill the χEFT constraints for the whole range of L studied, that is, $40 \leqslant L \leqslant 60$, since solutions outside the χEFT emerge for a value of $L = 60$. For $J = 30$ and $L = 60$ it turns out that large effective nucleon masses induce a softening of the neutron matter EoS for low-densities below the allowed χEFT band.

B. Mass and radius of neutron stars

Once the neutron matter EoS is known, we can study neutron stars by extending our analysis to β-stable neutron star matter. Therefore, the chemical potentials and the number densities of electrons, muons, protons, and neutrons in a neutron star core have to be related by the conditions

$$
\begin{aligned}
\mu_n &= \mu_p + \mu_e, \\
\mu_\mu &= \mu_e, \\
n_p &= n_e + n_\mu.
\end{aligned}
\tag{17}
$$

These relations, the Dirac equations for the nucleons (and electrons and muons), and the field equations for the mesonic fields σ, ω, and ρ are to be solved self-consistently for a given total nuclear density $n = n_p + n_n$. Once the chemical potential and the density of each species have been obtained at the given n, one can determine the energy density and pressure (EoS) of the neutron star matter for each density.

The mass M and the corresponding radius R of a nonrotating symmetrically spheric neutron star are obtained by solving the Tolman-Oppenheimer-Volkoff (TOV) equations

$$
\begin{aligned}
\frac{dM(r)}{dr} &= 4\pi \epsilon(r) r^2, \\
\frac{dp(r)}{dr} &= -\frac{[p(r) + \epsilon(r)][M(r) + 4\pi r^3 p(r)]}{r(r - 2M(r))}
\end{aligned}
\tag{18}
$$

in units $c = G = 1$. Here r is the radial coordinate and $M(r)$ is the mass enclosed by a radius r. By changing the value of the central pressure, one obtains the mass-radius relation of neutron stars using, for the core, the EoS described in the previous section.

For the inner and outer crust, we use the EoS at $T = 0.1$ MeV of the density-dependent relativistic mean-field model parametrization DD2 [59] in beta equilibrium as taken from the Compose online database [60]. The DD2 parametrization uses density-dependent couplings between the nucleons instead of meson (self-)interactions and is fitted to properties of nuclei. The crust EoS considers shell effects and the lattice energy as done for the outer crust in [61,62] extended to the inner crust of a neutron star. The DD2 equation of state at nonzero temperature is based on the thermodynamic ansatz
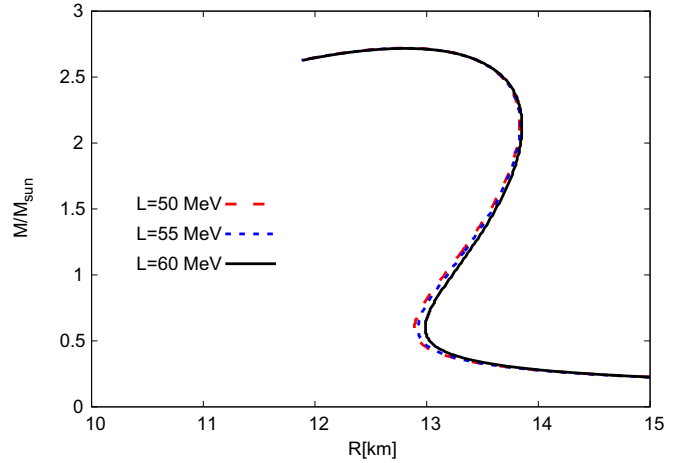

FIG. 5. Mass-radius relation for neutron stars for $J = 32$ and a fixed value of the effective mass $m^*/m = 0.60$, but for different values of the slope parameter, $50 \leqslant L \leqslant 60$.

of Ref. [63] and has been used in core-collapse supernova simulations in Ref. [64]. Note that the crust contributes to the overall size of a $1.4 M_\odot$ by ≈ 0.5 km.

Figure 5 shows the mass-radius relation for $J = 32$ and $m^*/m = 0.60$ for different values of the slope parameter $50 \leqslant L \leqslant 60$. Similar results are found for $J = 30$. We find that the $2M_\odot$ limit from pulsar mass measurements [5–7] is fulfilled for all mass-radius curves. In fact, the maximum mass is not sensitive to the variations of the slope parameter L, as already seen in Refs. [65,66]. The mixed interaction between ω and ρ mesons, with the coupling Λ_ω, governs the density dependence of the nuclear symmetry energy and, hence, the slope L around saturation density but turns out to be negligible at high densities, such as those found in the center of $2M_\odot$ neutron stars. This surprising finding is due to a delicate cancellation effect. At high densities the isoscalar vector field ω grows linearly with density, while the equation of motion for the isovector vector field ρ has a trivial solution for a ρ field growing inversely proportional to the density, i.e. $\rho \propto 1/n$, becoming negligible at high densities [see Eqs. (3)]. As for the radius of a $1.4 M_\odot$ neutron star, we find that it is nearly independent of the constrained value of L given by χEFT *ab initio* calculations. This is in contrast to some previous claims for a strong connection of the slope parameter with the radius of a neutron star, which, however, consider also a larger range for L [67–70]. As a consequence, all dependencies of isovector quantities on neutron star properties turn out to be small.

The effective nucleon mass, on the other hand, is responsible for the variation of both the maximum mass and the radius, as seen in Fig. 6. Due to the Hugenholtz-van-Hove theorem, the smaller the effective nucleon mass is, the stiffer the EoS is. Hence, small values of m^*/m lead to large neutron star masses above the $2M_\odot$ limit. However, recent constraints on the maximum mass coming from multimessenger observations of GW170817 [71,72] indicate that the maximum mass of a neutron star should be less than $\approx 2.16 M_\odot$. Thus, if these findings are confirmed with future observations of more GW
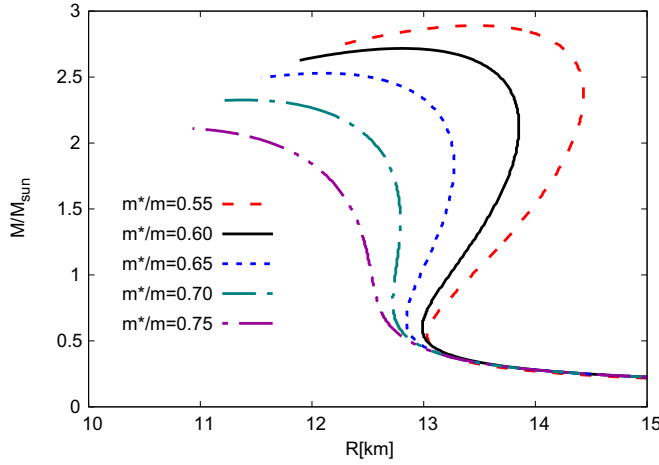
FIG. 6. Mass-radius relation for neutron stars for $J = 32$ MeV and $L = 60$ MeV for different values of m^*/m.

FIG. 7. Radius of $1.4M_\odot$ neutron star as a function of the slope parameter L for different effective nucleon masses for $J = 32$ MeV. At the right side of the figure, we show the upper limits on the radius of a $1.4M_\odot$ neutron star extracted from GW170817 by different groups [25,26,28,73].

events, this would indicate that our model for the high-dense phase is missing important contributions, such as the presence of hyperons or a phase transition that would soften the EoS and lead to the reduction of the maximum mass. With regard to the radii, small values of m^*/m give rise to large radii. However, the fact that our EoSs for neutron matter have to fulfill the χEFT constraints, that lead to soft EoSs in the low-density regime, gives rise to radii between 12.1 and 13.7 km for a $M = 1.4M_\odot$ neutron star, as seen in Table I.

In Fig. 7 we show the radius for a $1.4M_\odot$ neutron star as a function of L and m^*/m. We observe that changes in the effective nucleon mass have a stronger effect on the value of the radius as compared to variations in L. As pointed out in Ref. [68], there is a correlation of the radius of $1.4M_\odot$ stars with L. However, the constraints on our EoSs coming from χEFT do not allow for a wide variation of L (see Figs. 3 and 4). Thus, the variation of L is less important than the change of m^*/m for the determination of the radius of $1.4M_\odot$ star.

C. Tidal deformability

The recent detection of the gravitational wave event GW170817 coming from the binary neutron star merger by the LIGO and Virgo observatories [4] has posed constraints on the EoS through the tidal distortion during the inspiral phase. In a neutron star binary system, the tidal deformability
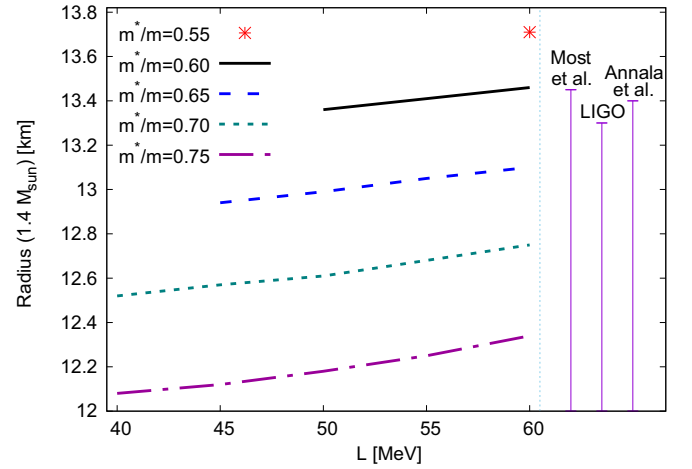
λ measures the induced quadrupole moment, Q_{ij}, of a star in response to the tidal field of the companion, $\mathcal{E}_{ij}$ [74,75]

$$Q_{ij} = -\lambda \mathcal{E}_{ij}. \tag{19}$$

The tidal deformability λ is related to the dimensionless $l = 2$ tidal Love number k_2 as

$$k_2 = \frac{3}{2}\lambda R^{-5}, \tag{20}$$

where R is the radius of the star. The tidal Love number can be calculated from

$$\begin{aligned}
k_2 = {} & \frac{8C^5}{5}(1 - 2C)^2[2 + 2C(y_R - 1) - y_R] \\
& \times \{2C[6 - 3y_R + 3C(5y_R - 8)] \\
& + 4C^3[13 - 11y_R + C(3y_R - 2) + 2C^2(1 + y_R)] \\
& + 3(1 - 2C)^2[2 - y_R + 2C(y_R - 1)]\ln(1 - 2C)\}^{-1},
\end{aligned} \tag{21}$$

with C being the compactness parameter ($C = M/R$). The quantity $y_R \equiv y(R)$ is obtained by solving, together with the TOV equations (18), the following differential equation

TABLE I. Central energy density, central pressure, radius, and dimensionless tidal deformability of a $1.4M_\odot$ neutron star for different values of m^*/m and for a slope parameter of $L = 60$ and a symmetry energy of $J = 32$. We also show the central energy density and the central pressure for a $2M_\odot$ neutron star as well as the maximum mass for the different values of the nucleon effective mass m^*/m and for $J = 32$ and $L = 60$.

m^*/m	$\epsilon_c(1.4M_\odot)\left[\frac{\text{MeV}}{\text{fm}^3}\right]$	$p_c(1.4M_\odot)\left[\frac{\text{MeV}}{\text{fm}^3}\right]$	$R_{1.4M_\odot}$[km]	$\Lambda_{1.4M_\odot}$	$\epsilon_c(2M_\odot)\left[\frac{\text{MeV}}{\text{fm}^3}\right]$	$p_c(2M_\odot)\left[\frac{\text{MeV}}{\text{fm}^3}\right]$	$M_{\text{max}}[M_\odot]$
0.55	268	32.2	13.9	1170	329	64.2	2.90
0.60	302	37.0	13.5	995	381	79.0	2.72
0.65	344	44.4	13.2	815	462	104	2.53
0.70	397	53.4	12.8	650	590	150	2.32
0.75	466	65.7	12.4	501	856	261	2.11

for y [76]

$$ry'(r) + y(r)^2 + y(r)e^{\lambda(r)}[1 + 4\pi r^2(p(r) - \epsilon(r))]$$
$$+ r^2 Q(r) = 0, \qquad (22)$$

where $e^{\lambda(r)} = (1 - \frac{2M(r)}{r})^{-1}$ is a metric function of a spherical star and

$$Q(r) = 4\pi e^{\lambda(r)}\left(5\epsilon(r) + 9p(r) + \frac{\epsilon(r) + p(r)}{c_s(r)^2}\right)$$
$$- 6e^{\lambda(r)}r^{-2} - [\nu'(r)]^2, \qquad (23)$$

with $\nu'(r)$ being the derivative of the $\nu(r)$ metric function

$$\nu'(r) = 2e^{\lambda(r)}\frac{M(r) + 4\pi p(r)r^3}{r^2}, \qquad (24)$$

and $c_s(r)^2 = dp/d\epsilon$ the squared speed of sound. The boundary condition of Eq. (22) is $y(0) = 2$. Once k_2 is known, the dimensionless tidal deformability Λ can then be determined by the relation

$$\Lambda = \frac{2k_2}{3C^5}. \qquad (25)$$

In Table I we show the dimensionless tidal deformability Λ for different values of m^*/m fixing $J = 32$ MeV and $L = 60$ MeV as in Fig. 6. Our value of Λ for $m^*/m > 0.65$ lies below the upper limit of $\Lambda \approx 800$ as given by Ref. [4]. We note that a recent reanalysis gives a somewhat lower limit of $\Lambda \lesssim 500$ within 90% credibility [27,28], so that only the case $m^*/m = 0.75$ would be compatible with GW170817. For completeness, we also show the radius, central energy density, and pressure of a $1.4M_\odot$ neutron star, as well as the central energy density and pressure at $2M_\odot$ together with the maximum mass reached for each value of m^*/m.

The constraints on the tidal deformability have also allowed for the determination of the statistically most probable radius of a $1.4M_\odot$ neutron star. Annala *et al.* [25] has recently concluded that the maximum radius of a $1.4M_\odot$ star is 13.60 km by combining the new stringent limits on tidal deformabilities with the existence of $2M_\odot$ stars using a a generic family of EoSs that interpolate between state-of-the-art theoretical results at low- and high-baryon density. Most *et al.* [26] have shown that a purely hadronic neutron star has $12.00 \leqslant R_{1.4M_\odot}(\text{km}) \leqslant 13.45$ with a 2-σ confidence level, with a most likely value of 12.39 km, by imposing constraints on the maximum mass ($M < 2.16M_\odot$) and on the dimensionless tidal deformability ($\Lambda < 800$ MeV) using 10^6 EoSs. Also, the recent article by the LIGO and Virgo scientific collaboration [28] has claimed that $10.50 \leqslant R_{1.4M_\odot}(\text{km}) \leqslant 13.30$ for EoSs which support maximum masses of $M \geqslant 1.97M_\odot$ at 90% credible level. In Ref. [27] a mass range of a binary neutron star merger with $1.1M_\odot \leqslant M \leqslant 1.6M_\odot$ has been studied, leading to $8.70 \leqslant R_{1.4M_\odot}(\text{km}) \leqslant 14.10$, with an average value of $R = 11.5$ km by means of a Bayesian parameter estimation, while in Ref. [73] it was found that GW170817 requires a radius of $R_{1.4M_\odot} < 13.6$ km. Our results for radii of a $1.4M_\odot$ star are compatible with all these analysis provided that $m^*/m > 0.60$, as seen in Fig. 7. Also similar results for $R_{1.4M_\odot}$ are found in theoretical analysis using different nonrelativistic and relativistic models constrained by the tidal

deformabilities [77–79]. We note that the lower limit on the radius found in the previous works is also fulfilled for all the cases studied in this paper.

In order to have radii below 13.5 km, we find that effective nucleon masses $m^*/m > 0.60$ are needed. Values of the effective mass above $m^*/m = 0.65$ have to be, though, taken with caution, as these values might not be compatible with experimental results on binding energies and charge radii of atomic nuclei [80]. The solution to this problem relies on the implementation of an isoscalar tensor term that will allow for effective masses $m^*/m > 0.60$ to be compatible with, for example, the large spin-orbit splitting of ^{16}O, which determines the magic numbers observed from nuclear binding [57]. This term is not relevant for the present relativistic Hartree mean-field calculation [81] of pure neutron matter and neutron star matter, but it would be of utmost relevance for the properties of finite nuclei, such as binding energies, charge radii, and spin-orbit splitting, as seen in Fig. 2 of Ref. [57]. Work along this line is beyond the scope of the present paper and is left for a future follow-up study.

V. CONCLUSIONS

We have studied the EoS in the inner core of neutron stars within the relativistic mean-field theory with the aim of fulfilling several recent astrophysical constraints, such as, the $2M_\odot$ neutron star mass limit [5–7] and the extraction of neutron star radii $\lesssim 13.5$ km from the recent analysis on tidal deformabilities of the GW170817 neutron star merger event [25–28,77–79].

The phenomenological model satisfies the saturation properties of nuclear matter together with constraints on low-density neutron matter coming from χEFT *ab initio* approaches [46]. These constraints are fulfilled by simultaneously fitting the isoscalar couplings to saturation properties (saturation density, energy per particle, and compressibility), while allowing for variations in the isovector parameters so as to reproduce the symmetry energy and its slope within reasonable theoretical and experimental limits [3,11,47–50].

We have found that the values of the symmetry energy $[30 \leqslant J \text{ (MeV)} \leqslant 32]$ and its slope $[40 \leqslant L \text{ (MeV)} \leqslant 60]$ that allow for a physical solution for the neutron matter EoS compatible with the χEFT are determined by the value of the nucleon effective mass $(0.55 \leqslant m^*/m \leqslant 0.75)$. It is indeed difficult to find a physical solution compatible with the χEFT results once the values for m^*/m and L are reduced (increased) simultaneously for a fixed value of J. A softening (hardening) of the EoS induced by a small (big) value of L competes with the stiffening (softening) of the EoS as we reduce (increase) the effective nucleon mass, leading to either a solution outside the allowed area from χEFT or the appearance of unstable solutions below saturation density.

With regard to the mass and radius of neutron stars, we have obtained that the effective nucleon mass turns out to be the dominant parameter controlling both the maximum mass and the radius of a neutron star. This is due to the fact that, on the one hand, the restricted range of L values coming from χEFT constraints does not allow for noticeable variations on the radius and, on the other hand, the isovector

TABLE II. Isoscalar coupling constants g_σ, g_ω, b, and c for different values of m^*/m, ranging from 0.55–0.75.

m^*/m	g_σ	g_ω	b	c
0.55	11.5529	13.5663	−0.00198839	−0.0028455
0.60	10.9935	12.7084	−0.00237445	−0.00315763
0.65	10.4291	11.7742	−0.0030843	−0.00368166
0.70	9.84608	10.7467	−0.00431483	−0.00434675
0.75	9.22731	9.59842	−0.00638591	−0.00426853

parameters turn out to be not relevant for the determination of the maximum mass, as seen in Refs. [65,66]. Large values of m^*/m induce small masses and radii, as expected from the Hugenholtz-van-Hove theorem. Thus, effective nucleon masses of $m^*/m > 0.6$ are needed in order to reproduce $2M_\odot$ observations and have radii compatible with recent astrophysical determinations [14–16,18–20,22,23,82,83], that are corroborated by the analysis on tidal deformabilities of the GW170817 event [25–28,77–79]. In fact, our values of the dimensionless tidal deformability are within the 90% confidence level for $m^*/m > 0.65$ at $J = 32$ and $L = 60$. Note, however, that the effective nucleon mass has to be reconciled

with the binding energies and charge radius of atomic nuclei [80].

In the near future, apart from the expected detection of gravitational-wave events from other neutron star binary systems, high-precision x-ray space missions, such as the ongoing NICER [29] and the eXTP [30], will shed some more light on the properties of matter inside neutron stars by offering simultaneous measurements of their masses and radii [31].

APPENDIX: ISOSCALAR AND ISOVECTOR COUPLING CONSTANTS

In this Appendix we show the values of the coupling constants in the isoscalar and isovector sectors used throughout this work. The isoscalar coupling constants (g_σ, g_ω, b, and c) are given in Table II for the different values of m^*/m, ranging

TABLE III. Isovector coupling constants g_ρ and Λ_ω for $J = 30$ and for different values of L. We also show whether the set of parameters gives a physical solution inside the χEFT band (marked as $*$), an unphysical one showing unstable regions (indicated as $+$) or outside the χEFT band (depicted by $\times$). The analysis of the possible solutions is shown in Fig. 3.

L (MeV)	m^*/m	g_ρ	Λ_ω	Solution
40	0.55	34.168	0.0532996	$+$
40	0.60	14.5669	0.0493023	$\times$
40	0.65	12.4947	0.0465416	$*$
40	0.70	11.3062	0.0581025	$*$
40	0.75	10.8953	0.0754378	$*$
45	0.55	19.5876	0.0490439	$+$
45	0.60	12.7990	0.0449062	$*$
45	0.65	11.2725	0.0458165	$*$
45	0.70	10.6459	0.0519231	$*$
45	0.75	10.3644	0.0668463	$*$
50	0.55	15.1512	0.0447882	$\times$
50	0.60	11.5498	0.0405102	$*$
50	0.65	10.5223	0.0408349	$*$
50	0.70	10.0892	0.0457436	$*$
50	0.75	9.90415	0.0582548	$*$
55	0.55	12.7974	0.0405326	$*$
55	0.60	10.607	0.0361141	$*$
55	0.65	9.90434	0.0358532	$*$
55	0.70	9.61159	0.0395641	$*$
55	0.75	9.50027	0.0496634	$*$
60	0.55	11.2825	0.0362769	$*$
60	0.60	9.86283	0.0317181	$\times$
60	0.65	9.38387	0.0308716	$\times$
60	0.70	9.19598	0.0333846	$\times$
60	0.75	9.14208	0.0410719	$\times$

TABLE IV. The same as Table III, but for $J = 32$. The analysis of the possible solutions is shown in Fig. 4.

L (MeV)	m^*/m_N	g_ρ	Λ_ω	Solution
40	0.55	21.8033	0.0416554	$+$
40	0.60	14.5748	0.04026	$\times$
40	0.65	12.7802	0.0429272	$\times$
40	0.70	11.9943	0.0504747	$*$
40	0.75	11.6139	0.0670394	$*$
45	0.55	17.2734	0.0386202	$+$
45	0.60	13.2057	0.0370172	$\times$
45	0.65	11.9513	0.0391607	$*$
45	0.70	11.3799	0.045714	$*$
45	0.75	11.107	0.0603224	$*$
50	0.55	14.745	0.0355851	$+$
50	0.60	12.1617	0.0337743	$*$
50	0.65	11.2653	0.0353941	$*$
50	0.70	10.8512	0.0409534	$*$
50	0.75	10.6612	0.0536054	$*$
55	0.55	13.0772	0.0325499	$\times$
55	0.60	11.3317	0.0305315	$*$
55	0.65	10.6852	0.0316276	$*$
55	0.70	10.3899	0.0361928	$*$
55	0.75	10.2651	0.0468884	$*$
60	0.55	11.8716	0.0295148	$*$
60	0.60	10.6513	0.0272887	$*$
60	0.65	10.1865	0.0278611	$*$
60	0.70	9.9829	0.0314321	$*$
60	0.75	9.9101	0.0401714	$*$

from 0.55–0.75. We take $m = 939$ MeV, $m_\omega = 783$ MeV, and $m_\sigma = 550$ MeV for the masses of the nucleon, ω and σ mesons, respectively. The coupling constant ζ is set to zero.

The isovector coupling constants g_ρ and Λ_ω are shown in Tables III and IV for $J = 30$ MeV and $J = 32$ MeV, respectively, and for different values of L, such that $40 \leqslant L$ (MeV) $\leqslant 60$ MeV. In these two tables we also show whether the corresponding EoS is physical and inside the allowed area coming from χEFT constraints (marked as $\ast$), or unphysical (indicated as $+$) or outside the χEFT band (depicted by $\times$).

---

[1] J. M. Lattimer and M. Prakash, Science **304**, 536 (2004).

[2] J. M. Lattimer and M. Prakash, Phys. Rep. **442**, 109 (2007).

[3] M. Oertel, M. Hempel, T. Klahn, and S. Typel, Rev. Mod. Phys. **89**, 015007 (2017).

[4] B. Abbott *et al.* (LIGO Scientific Collaboration and Virgo Collaboration), Phys. Rev. Lett. **119**, 161101 (2017).

[5] P. Demorest, T. Pennucci, S. Ransom, M. Roberts, and J. Hessels, Nature (London) **467**, 1081 (2010).

[6] J. Antoniadis, P. C. Freire, N. Wex, T. M. Tauris, R. S. Lynch, M. H. van Kerkwijk, M. Kramer, C. Bassa, V. S. Dhillon, T. Driebe, J. W. T. Hessels, V. M. Kaspi, V. I. Kondratiev, N. Langer, T. R. Marsh, M. A. McLaughlin, T. T. Pennucci, S. M. Ransom, I. H. Stairs, J. van Leeuwen, J. P. W. Verbiest, and D. G. Whelan, Science **340**, 1233232 (2013).

[7] E. Fonseca *et al.*, Astrophys. J. **832**, 167 (2016).

[8] J. P. W. Verbiest, M. Bailes, W. van Straten, G. B. Hobbs, R. T. Edwards, R. N. Manchester, N. D. R. Bhat, J. M. Sarkissian, B. A. Jacoby, and S. R. Kulkarni, Astrophys. J. **679**, 675 (2008).

[9] F. Ozel, G. Baym, and T. Guver, Phys. Rev. D **82**, 101301 (2010).

[10] V. Suleimanov, J. Poutanen, M. Revnivtsev, and K. Werner, Astrophys. J. **742**, 122 (2011).

[11] J. M. Lattimer and Y. Lim, Astrophys. J. **771**, 51 (2013).

[12] A. W. Steiner, J. M. Lattimer, and E. F. Brown, Astrophys. J. **765**, L5 (2013).

[13] S. Bogdanov, Astrophys. J. **762**, 96 (2013).

[14] T. Guver and F. Ozel, Astrophys. J. **765**, L1 (2013).

[15] S. Guillot, M. Servillat, N. A. Webb, and R. E. Rutledge, Astrophys. J. **772**, 7 (2013).

[16] J. M. Lattimer and A. W. Steiner, Astrophys. J. **784**, 123 (2014).

[17] J. Poutanen, J. Nättilä, J. J. E. Kajava, O.-M. Latvala, D. Galloway, E. Kuulkers, and V. Suleimanov, Mon. Not. R. Astron. Soc. **442**, 3777 (2014).

[18] C. O. Heinke *et al.*, Mon. Not. R. Astron. Soc. **444**, 443 (2014).

[19] S. Guillot and R. E. Rutledge, Astrophys. J. **796**, L3 (2014).

[20] F. Ozel, D. Psaltis, T. Guver, G. Baym, C. Heinke, and S. Guillot, Astrophys. J. **820**, 28 (2016).

[21] F. Ozel and D. Psaltis, Astrophys. J. **810**, 135 (2015).

[22] F. Ozel and P. Freire, Annu. Rev. Astron. Astrophys. **54**, 401 (2016).

[23] J. M. Lattimer and M. Prakash, Phys. Rep. **621**, 127 (2016).

[24] A. W. Steiner, C. O. Heinke, S. Bogdanov, C. Li, W. C. G. Ho, A. Bahramian, and S. Han, Mon. Not. R. Astron. Soc. **476**, 421 (2018).

[25] E. Annala, T. Gorda, A. Kurkela, and A. Vuorinen, Phys. Rev. Lett. **120**, 172703 (2018).

[26] E. R. Most, L. R. Weih, L. Rezzolla, and J. Schaffner-Bielich, Phys. Rev. Lett. **120**, 261103 (2018).

[27] S. De, D. Finstad, J. M. Lattimer, D. A. Brown, E. Berger, and C. M. Biwer, Phys. Rev. Lett. **121**, 091102 (2018).

[28] B. P. Abbott *et al.* (LIGO Scientific Collaboration and Virgo Collaboration), Phys. Rev. Lett. **121**, 161101 (2018).

[29] Z. Arzoumanian, K. C. Gendreau, C. L. Baker, T. Cazeau, P. Hestnes, J. W. Kellogg, S. J. Kenyon, R. P. Kozon, K.-C. Liu, S. S. Manthripragada, C. B. Markwardt, A. L. Mitchell, J. W. Mitchell, C. A. Monroe, T. Okajima, S. E. Pollard, D. F. Powers, B. J. Savadkin, L. B. Winternitz, P. T. Chen, M. R. Wright, R. Foster, G. Prigozhin, R. Remillard, and J. Doty, Proc. SPIE, **9144**, 914420 (2014).

[30] S. N. Zhang *et al.* (eXTP Collaboration), Proc. SPIE-Int. Soc. Opt. Eng. **9905**, 99051Q (2016).

[31] A. L. Watts *et al.*, Rev. Mod. Phys. **88**, 021001 (2016).

[32] B. D. Serot and J. D. Walecka, Adv. Nucl. Phys. **16**, 1 (1986).

[33] H. Mueller and B. D. Serot, Nucl. Phys. A **606**, 508 (1996).

[34] B. D. Serot and J. D. Walecka, Int. J. Mod. Phys. E **6**, 515 (1997).

[35] N. K. Glendenning, *Compact Stars: Nuclear Physics, Particle Physics, and General Relativity*, 2nd ed. (Springer, New York, 2000).

[36] F. J. Fattoyev and J. Piekarewicz, Phys. Rev. C **82**, 025805 (2010).

[37] W.-C. Chen and J. Piekarewicz, Phys. Rev. C **90**, 044305 (2014).

[38] F. Weber and M. K. Weigel, Nucl. Phys. A **493**, 549 (1989).

[39] C. J. Horowitz and J. Piekarewicz, Phys. Rev. Lett. **86**, 5647 (2001).

[40] D. Chatterjee and I. Vidana, Eur. Phys. J. A **52**, 29 (2016).

[41] F. Weber, Prog. Part. Nucl. Phys. **54**, 193 (2005).

[42] M. Alford, D. Blaschke, A. Drago, T. Klähn, G. Pagliara, and J. Schaffner-Bielich, Nature (London) **445**, E7 (2006).

[43] S. Weissenborn, I. Sagert, G. Pagliara, M. Hempel, and J. Schaffner-Bielich, Astrophys. J. **740**, L14 (2011).

[44] M. Buballa, V. Dexheimer, A. Drago, E. Fraga, P. Haensel, I. Mishustin, G. Pagliara, J. Schaffner-Bielich, S. Schramm, A. Sedrakian, and F. Weber, J. Phys. G **41**, 123001 (2014).

[45] A. Zacchi, R. Stiele, and J. Schaffner-Bielich, Phys. Rev. D **92**, 045022 (2015).

[46] C. Drischler, A. Carbone, K. Hebeler, and A. Schwenk, Phys. Rev. C **94**, 054307 (2016).

[47] B.-A. Li and X. Han, Phys. Lett. B **727**, 276 (2013).

[48] X. Roca-Maza, X. Viñas, M. Centelles, B. K. Agrawal, G. Colo', N. Paar, J. Piekarewicz, and D. Vretenar, Phys. Rev. C **92**, 064304 (2015).

[49] G. Hagen *et al.*, Nature Phys. **12**, 186 (2016).

[50] J. Birkhan, M. Miorelli, S. Bacca, S. Bassauer, C. A. Bertulani, G. Hagen, H. Matsubara, P. von Neumann-Cosel, T. Papenbrock, N. Pietralla, V. Y. Ponomarev, A. Richter, A. Schwenk, and A. Tamii, Phys. Rev. Lett. **118**, 252501 (2017).

[51] J. Boguta and A. R. Bodmer, Nucl. Phys. A **292**, 413 (1977).

[52] J. Boguta and H. Stöcker, Phys. Lett. B **120**, 289 (1983).

[53] D. H. Youngblood, H. L. Clark, and Y. W. Lui, Phys. Rev. Lett. **82**, 691 (1999).

[54] C. J. Horowitz and J. Piekarewicz, Phys. Rev. C **64**, 062802 (2001).

[55] B. G. Todd-Rutel and J. Piekarewicz, Phys. Rev. Lett. **95**, 122501 (2005).

[56] S. Shlomo, V. M. Kolomietz, and G. Colò, Eur. Phys. J. A **30**, 23 (2006).

[57] R. J. Furnstahl and B. D. Serot, Nucl. Phys. A **673**, 298 (2000).

[58] J. Boguta, Phys. Lett. B **106**, 250 (1981).

[59] S. Typel, G. Röpke, T. Klähn, D. Blaschke, and H. H. Wolter, Phys. Rev. C **81**, 015803 (2010).

[60] https://compose.obspm.fr.

[61] G. Baym, C. Pethick, and P. Sutherland, Astrophys. J. **170**, 299 (1971).

[62] S. B. Rüster, M. Hempel, and J. Schaffner-Bielich, Phys. Rev. C **73**, 035804 (2006).

[63] M. Hempel and J. Schaffner-Bielich, Nucl. Phys. A **837**, 210 (2010).

[64] T. Fischer, M. Hempel, I. Sagert, Y. Suwa, and J. Schaffner-Bielich, Eur. Phys. J. A **50**, 46 (2014).

[65] L. Tolos, M. Centelles, and A. Ramos, Astrophys. J. **834**, 3 (2017).

[66] L. Tolos, M. Centelles, and A. Ramos, Pub. Astron. Soc. Aust. **34**, e065 (2017).

[67] F. J. Fattoyev, J. Carvajal, W. G. Newton, and B.-A. Li, Phys. Rev. C **87**, 015806 (2013).

[68] N. Alam, B. K. Agrawal, M. Fortin, H. Pais, C. Providencia, A. R. Raduta, and A. Sulaksono, Phys. Rev. C **94**, 052801 (2016).

[69] Z.-Y. Zhu, E.-P. Zhou, and A. Li, Astrophys. J. **862**, 98 (2018).

[70] Y. Lim and J. W. Holt, Phys. Rev. Lett. **121**, 062701 (2018).

[71] B. Margalit and B. D. Metzger, Astrophys. J. **850**, L19 (2017).

[72] L. Rezzolla, E. R. Most, and L. R. Weih, Astrophys. J. **852**, L25 (2018).

[73] I. Tews, J. Margueron, and S. Reddy, Phys. Rev. C **98**, 045804 (2018).

[74] T. Hinderer, Astrophys. J. **677**, 1216 (2008).

[75] T. Hinderer, B. D. Lackey, R. N. Lang, and J. S. Read, Phys. Rev. D **81**, 123016 (2010).

[76] S. Postnikov, M. Prakash, and J. M. Lattimer, Phys. Rev. D **82**, 024016 (2010).

[77] B. Kumar, S. K. Patra, and B. K. Agrawal, Phys. Rev. C **97**, 045806 (2018).

[78] F. J. Fattoyev, J. Piekarewicz, and C. J. Horowitz, Phys. Rev. Lett. **120**, 172702 (2018).

[79] T. Malik, N. Alam, M. Fortin, C. Providência, B. K. Agrawal, T. K. Jha, B. Kumar, and S. K. Patra, Phys. Rev. C **98**, 035804 (2018).

[80] P. G. Reinhard, Rept. Prog. Phys. **52**, 439 (1989).

[81] H. Sagawa and G. Colò, Prog. Part. Nucl. Phys. **76**, 76 (2014).

[82] J. M. Lattimer and A. W. Steiner, Eur. Phys. J. A **50**, 40 (2014).

[83] J. Nättilä, A. W. Steiner, J. J. E. Kajava, V. F. Suleimanov, and J. Poutanen, Astron. Astrophys. **591**, A25 (2016).